A biodistribution study of PEGylated PCL-based nanoparticles in C57BL/6 mice bearing B16/F10 melanoma

M Lupi[1,4], C Colombo[1,2,4], R Frapolli[1], R Ferrari[2], L Sitia[1], L Dragoni[2], E Bello[1], S A Licandro[1], F Falcetta[1], P Ubezio[1], P Bigini[1], M Salmona[1], M D'Incalci[1], M Morbidelli[3] and D Moscatelli[2]

[1] IRCCS—Istituto di Ricerche Farmacologiche Mario Negri, Via La Masa 19, I-20156, Milano, Italy

[2] Department of Chemistry, Materials and Chemical Engineering 'Giulio Natta,' Politecnico di Milano, Via Luigi Mancinelli 7, I-20131 Milano, Italy

[3] Institute for Chemical and Bioengineering, Department of Chemistry and Applied Biosciences, ETH Zurich, Wolfgang-Pauli Str. 10 8093, Zurich, Switzerland

[4] These authors contributed equally to this work.
E-mail: davide.moscatelli@polimi.it

Received 10 April 2014, revised 10 June 2014
Accepted for publication 23 June 2014
Published 30 July 2014

1. Introduction

The use of nanotechnology as a tool for the delivery of pharmaceuticals in a safer way (nanomedicine) is closely related to the advancement in the development of nanocarriers such as liposomes, micelles and polymer nanoparticles (NPs) as drug delivery systems [1]. Latter nanocarriers have been widely studied due to their excellent biocompatibility, tunable proprieties and ability to convey a wide variety of pharmaceuticals [2–4]. In general, a drug delivery system has to be able to avoid recognition by the macrophages and to accumulate preferentially in the target organ. The first feature is usually obtained with the addition of poly(ethylene glycol) (PEG), which is known to prevent opsonization and thus increase the half-life of the injected particles in the bloodstream [5, 6]. The targeting of specific organs or tumors can

be achieved with surface functionalization with ligands such as folic acid [7–9], monoclonal antibodies [10, 11] and epidermal growth factors, which bind specific receptors and maximize the cellular uptake [12]. Another way to achieve preferential targeting in certain solid tumors is to exploit their leaky vasculature, which is a long-known characteristic [13] that can lead to a greater accumulation due to a phenomenon known as the enhanced permeability and retention effect (EPR) [14]. However, despite the high number of carriers that rely on the EPR effect to accumulate in the tumor, only a slight few applications have reached clinical use [15]. This discrepancy is attributable to many factors, among which is a lack of deep understanding on how nanocarriers behave once injected in the body [16]. In addition, attention is often solely focused on the amount of NPs that reach the tumor and not on their overall biodistribution in the different organs [17]. NP characteristics, such as dimension, surface charge and functionalization, can greatly affect their behavior post injection in terms of both their biodistribution and their interaction with the body [18, 19]. Therefore, preclinical studies aimed at the understanding of NP biodistribution are a relevant step in their development; these tests are usually carried out by making fluorescent NPs [20], for example, by using a dye that can be either covalently bound [21] or simply loaded into the carrier [22, 23]. Another way revolves around the use of radiolabeled substances [24–27].

In this work, the biodistribution of PEGylated polymer nanoparticles based on poly ε-caprolactone (PCL) and produced through emulsion free radical polymerization is studied. These NPs are synthesized starting from PCL-based oligomers obtained through the ring opening polymerization (ROP) of ε-caprolactone, and they are initiated by 2-hydroxy ethyl methacrylate (HEMA), using tin octoate as a catalyst [28]. The final products are PCL-based oligomers with a controllable length that are functionalized with a vinyl bond (HEMA-CL_n), which can be employed in a subsequent free radical polymerization. NPs are produced by copolymerizing these oligomers with a PEGylated hydroxy ethyl methacrylate (HEMA-PEG) macromonomer through a surfactant free monomer-starved semi-batch emulsion polymerization (MSSEP) process [29]. The final products of this synthetic route are NPs composed by copolymers characterized by a poly(HEMA) backbone with PCL-grafted chains confined in the core and PEG chains mainly localized in the outer shell. The versatility of the MSSEP process allows an easy functionalization of the NPs via a terpolymerization, with a fluorescent methacrylate monomer obtained by conjugating rhodamine B (RhB) and HEMA with dicyclohexil carbodiimide (DCC) [30].

These NPs have already been successfully employed with hydrogels in a localized treatment for spinal cord injury [31]; here, the presence of a dye covalently bound to the NPs allows the precise quantification of their cellular uptake *in vitro*, as well as in-depth study concerning their systemic *in vivo* biodistribution. The degradation of the produced NPs was followed in a cell medium at 37 °C, and NP biocompatibility was evaluated by incubating B16/F10 mouse melanoma cells with different NP concentrations for 24 h. The obtained results showed slight cytotoxic effects only for high polymer concentrations, while the cellular uptake that combined the absolute cell count and the plate fluorimetry was quantitatively studied [32]. *In vivo* NP biodistribution was studied in mice bearing the same tumor; this study was aimed at fulfilling the total mass balance. At different times, after intravenous (i.v.) injection of the NPs, the plasma, tumor and the major organs, as well as the urine and feces, were fluorometrically measured in order to quantify the amount of the RhB present. The calibration curves, obtained by serial dilutions of NPs in the fluids (plasma and urine) and in the homogenized organs, allowed the measurement of the NP concentration. In particular, it was possible to determine the fate of 86% of the injected NPs, even after 72 h, with an almost time-constant NP accumulation in the tumor equal to about 3% of the injected dose per gram of tissue. For the adopted NPs, it was possible to calculate a half-life in the blood tream equal to about 30 min. Finally, *ex vivo* confocal microscopy analyses were performed to study the cellular localization of the NPs in different organs and then to obtain further details about their *in vivo* behaviour, which confirmed their ability to be internalized in tumor cells *in vivo*.

2. Materials and methods

2.1. Materials

For macromonomer production and NP synthesis ε-caprolactone (CL, 99%), 2-hydroxyethyl methacrylate (HEMA, ⩾99%), 2-ethylhexanoic acid tin(II) salt ($Sn(Oct)_2$, ~95%), potassium persulfate (KPS, ⩾99%), poly(ethylene glycol) methyl ether methacrylate (HEMA-PEG_{19}, molecular weight: ca. 950 Da), rhodamine B (RhB, > 95%), N,N′-dicyclohexyl carbodiimide (DCC, 99%), acetonitrile (anhydrous, >99.8%) and 4-(dimethylamino) pyridine (DMAP, >99%) were purchased from Sigma Aldrich and used without further treatment. Phosphate buffered saline solution (PBS, Biowest, Nuaillé, France), 0.05% trypsin-0.02% EDTA in PBS solution (Biowest), a cell medium composed of high glucose DMEM (Biowest) and supplemented with 10% fetal bovine serum (Lonza, Basel, Switzerland) and 1% L-glutamine (Biowest) were all used without further treatment. For the pharmacokinetic study RIPA buffer, paraformaldehyde (powder, 95%), Hoechst 33 258 and Sucrose (⩾99.5%) were purchased from Sigma Aldrich. n-pentane (⩾99%) was purchased from Carlo Erba Reagents.

2.2. Nanoparticle synthesis and characterization

The HEMA-CL_3 macromonomer was synthesized through the ROP following a procedure reported in literature [28]. Briefly, the reaction was carried out in bulk conditions without using any solvent. 10 g of CL were first heated up in a stirred flask at 130 ± 1 °C with the temperature controlled by an external oil bath. A mixture of $Sn(Oct)_2$ (30 mg) and HEMA (3.8 g) was prepared and left under continuous magnetic stirring at room temperature until complete dissolution of the $Sn(Oct)_2$. This mixture was then added to the CL (CL/HEMA molar ratio

equal to 3) to initiate the reaction, which had been carried out for 2 h. The reaction product (HEMA-CL_3) was refrigerated at 4 °C while waiting for further use. The macromonomer average molecular weight (MW) was characterized by proton nuclear magnetic resonance (^{1}H-NMR); the instrument details, together with the macromonomer characterization, are reported in the appendixes section (figure A1).

The fluorescent HEMA-RhB monomer that was used for NP detection had been synthesized using a procedure reported in literature [30]. 1 g of RhB together with 0.325 g of HEMA were dissolved in 30 ml acetonitrile in a beaker under magnetic stirring at room temperature. 0.43 g of DCC and 13 mg of DMAP were dissolved in 20 ml of acetonitrile; this solution was added dropwise to the previous solution within 20 min. The reaction was then carried out in the dark at 40 °C under magnetic stirring for 24 h and then quenched in an ice bath for 10 min. Dicyclohexylurea, the side product of the coupling reaction, was eliminated from the solution through filtration, and finally, acetonitrile was removed using a rotatory vacuum.

The MSSEP of the produced macromonomers was carried out in a 50 ml three-necked glass flask, as described elsewhere [29, 32]. 0.5 g of HEMA-PEG_{19} were added to 45 ml of distilled water, and the solution was heated up to 80 °C; the inert atmosphere was obtained through nitrogen-vacuum cycles. 0.02 g of KPS, dissolved in 2.5 ml of distilled water, were added to the purged solution. After that, 2 g of HEMA-CL_3 were injected with a rate of 2 ml h^{-1} using a syringe pump (Model NE-300, New Era Pump Systems, US), together with the fluorescent HEMA-RhB monomer (which represent the 0.1% wt of the overall polymer). The reaction ran for 3 h. The solid contents of all the final latexes was equal to 2.5 g (5% wt/wt). The data about the size and the particle size distribution (PSD) of the NP dispersions have been determined through dynamic light scattering (DLS) measurements (Malvern, Zetanano ZS). All of the reported data are an average value of three measurements of the same sample.

The NP stability in the biological media was tested as follows: 1 ml of diluted NP solution (0.1% wt/wt) was added to 1 ml of cell medium containing 10% of fetal bovine serum [33]. The solution was maintained at 37 ± 0.1 °C in a heating block, and the NP size was measured after 72 h (DLS); additional information is shown in the appendixes.

2.3. Cell culture

B16/F10 mouse melanoma cells were grown as monolayers in T25 tissue flasks (Iwaki, BibbySterilin, Staffordshire, UK) in high glucose DMEM supplemented with 10% fetal bovine serum and 1% L-glutamine, maintained at 37 °C in a humidified atmosphere containing 5% CO_2 and routinely subcultured twice weekly; the cells were detached using 1 ml of a solution containing 0.05% trypsin and 0.02% EDTA dissolved in PBS. Trypsin activity was stopped using a culture medium. All of the detached cells were counted using a Coulter Counter ZM (Coulter Electronics, Harpenden, UK).

2.4. In vitro cytotoxicity and cellular uptake

B16/F10 cells were seeded in 6-well plates (Iwaki) at the concentration of 10 000 cell ml^{-1}. 24 h after seeding, the cells were incubated with NPs at different concentrations (1.6×10^{10}; 8.0×10^{10}; 4×10^{11}; 2×10^{12} #NPs ml^{-1}).

After 1 h or 24 h of exposure to NPs cells were trypsinized and counted with the Coulter Counter ZM. The detection of cell fluorescence and the quantification of the internalized NPs was done as previously described [34]; more information about the quantification is found in the appendixes. Three replicated samples for each concentration and for each time were analyzed.

2.5. Animal model

Female C57BL/6 mice, 7 weeks old, were obtained from Harlan Laboratories (Udine, Italy). They were maintained under specific pathogen-free conditions in the Institute's Animal Care Facilities, which meet international standards; they were regularly checked by a certified veterinarian who is responsible for health monitoring, animal welfare supervision, experimental protocols and procedures revision. Procedures involving animals and their care were reviewed and approved by the IRFMN Animal Care and Use Committee (IACUC), which includes members 'ad hoc' for ethical issues, and were conducted in conformity with institutional guidelines that are in compliance with national (Legislative Decree 116 of Jan. 27, 1992 Authorization n.169/94-A issued Dec. 19, 1994 by Ministry of Health) and international laws and policies (EEC Council Directive 86/609, OJ L 358. 1, Dec. 12, 1987; Standards for the Care and Use of Laboratory Animals, United States National Research Council, Statement of Compliance A5023-01, Nov. 6, 1998.).

10^6 B16/F10 cells were injected subcutaneously in the right flank of the mice. The growing tumor masses were measured with the aid of a Vernier caliper, and the tumor weights were calculated by the formula $\text{length}*\frac{\text{width}^2}{2}$ ($1\ mm^3 = 1$ g). When the tumor load reached a weight of about 300–500 mg, the mice were randomized in the experimental groups.

2.6. Pharmacokinetic study and histological analysis

1.5×10^{13} #NPs ml^{-1} were administered i.v. at the dose volume of 10 ml kg^{-1} (the injected dose (ID) was, on average, 3.14×10^{12} #NPs, given at 0.206 ml per mouse). Blood samples were collected in heparinized tubes from the retro-orbital plexus under isoflurane anesthesia at 15 and 30 min, 1 h, 3 h, 6 h, 24 h, 72 h, 120 h and 7 d after treatment. Blood samples were centrifuged at 4000 rpm for 15 min to separate the plasma. For the evaluation of the NPs distributed in the organs, three mice for each time period were sacrificed by cervical dislocation, and the liver, kidneys, spleen, heart, lungs, brain and tumor were collected. All of the samples were immediately frozen in dry ice and stored at −20 °C until analyzed. On the day of the analysis, the tissues were weighed and homogenized in a RIPA Buffer (1:3 w v^{-1}); then, the samples were centrifuged at 1200 rpm for 10 min, and 100 μl

of the supernatant or 100 μl of plasma were loaded in each well of a 96-well plate (Iwaki) for microplate reader analysis of the fluorescence signals.

Feces and urine were collected from the mice housed in metabolic cages for 24 h and 48 h from NP injection and were stored at −20 °C. For the microplate reader analysis, 100 μl well^{-1} of urine were loaded in triplicate in a 96-well plate, while the feces were weighed and homogenized in a RIPA buffer (1:3 w v^{-1}) and then processed like the other tissues.

Standard calibration curves were prepared in control tissues, plasma, feces and urine, considering serial dilution of the original latex, starting from 1:10 (v/v) of the initial concentration, loading 100 μl well^{-1} of suspension in a 96-well plate. The analysis of the fluorescence signals was performed using a multimode microplate reader (TECAN) with the following instrumental setting: $\lambda_{exc} = 530$ nm, $\lambda_{em} = 585$ nm and gain 70 for the plasma and tissues and gain 100 for the feces and urine. The fluorescence signal detected by the instrument was plotted as a function of the number of NPs in each well, which was derived in consideration of the concentration in the NP suspension and the dilutions applied. The fluorescence was proportional to the number of NPs, and from the linear fit of the data, it was possible to derive the quantity of the NPs corresponding to a fluorescence unit detected by the microplate reader in the fixed instrumental setting (figure D1 in the appendixes). Using the tissue-specific calibration scale, the absolute concentration of the NPs in each homogenate was derived from the fluorescence measure; then, the concentration in the organ was calculated (as #NPs/g) by taking into account the final homogenate volume and the weight of the organ. Finally, the NP concentration was rescaled as percentage of the injected dose (% ID/g). The overall number of NPs in the plasma was calculated by assuming a plasma percentage of 55% and a blood volume of 1.2 ml.

For histological analyses, three animals belonging to the group of mice that were sacrificed at 3 h and 72 h after NP administration were selected. In addition, three animals that received the same volume of saline solution were included as an internal control. To ensure optimal integrity of the tissues, the animals were perfused by transcardiac perfusion with 0.1 M PBS pH 7.4, followed by 4% paraformaldehyde in PBS under deep anesthesia with an overdose of ketamine (75 mg kg^{-1}) and metodimine (1 mg kg^{-1}). Immediately after perfusion, the liver, spleen, kidneys and tumors were rapidly removed and post-fixed for 4 h in the same fixative (4 °C). All of the tissues were dehydrated and cryoprotected with serial steps in 20% and 30% sucrose in 0.1 M PBS at 4 °C until they sank; then, they were frozen in n-pentane at −45 °C and stored at −80 °C until analysis. Histological analyses were performed by incubating cryostat serial sections (30 μm of thickness) with the vital nuclear dye Hoechst 33 258 (2 μg ml^{-1}, 35 min, RT). Sections were covered with an aqueous mounting medium for use with fluorescent dye-stained tissues (Fluoromont, Sigma Aldrich) and sealed with a glass coverslip. The slides were visualized by an Olympus Fluoview microscope BX61 (Tokyo, Japan) with confocal system FV500 equipped by specific lasers with $\lambda_{exc} = 405$ nm for Hoechst 33 258, $\lambda_{exc} = 448$ nm to unveil the tissues autofluorescence and $\lambda_{exc} = 546$ nm to visualize the RhB.

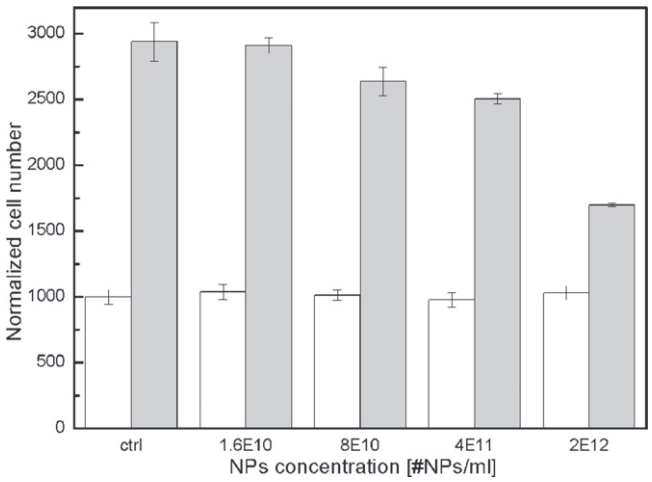

Figure 1. Proliferation of B16/F10 cells exposed to different concentrations of NPs (ranging from 1.6×10^{10} to 2×10^{12} #NPs ml^{-1}). The cells were counted after 1 h (white bars) and 24 h (grey bars) of exposure to the NPs (cell number normalized over the control at 1 h and set equal to 1000). The columns and error bars represent the mean and standard deviation of three replicates.

3. Results and discussion

3.1. Nanoparticle synthesis

PEGylated PCL-based NPs were synthesized by a combination of ROP and MSSEP processes, as already reported, without using any organic solvent or surfactant [29]. In particular, the ROP allowed us to obtain a macromonomer constituted by a HEMA molecule functionalized with three CL units (HEMA-CL_3), which was subsequently copolymerized to HEMA-PEG_{19} to give monodispersed, surfactant free NPs of 138 nm with a low polydispersity index (0.118) and ζ potential of −2.6 mV. In order to prove the stability of these NPs in biological fluids, the main physical-chemical parameters described above were monitored for 72 h in a cell culture medium. DLS analysis did not reveal any significant alteration in terms of both size and polydispersity for the whole duration of the experiment (see figure B1 in the appendixes), meaning that no aggregation or degradation took place.

3.2. Biocompatibility: in vitro studies

The interaction between the cells and the NPs was studied *in vitro* by incubating B16/F10 cells with different NP concentrations. The absolute cell count after 1 h and 24 h of incubation with the NPs showed that only the cells exposed to the highest concentration (2×10^{12} #NPs ml^{-1}) were not able to proliferate like the controls (figure 1). For all of the other samples, the number of cells after 24 h of incubation was, at maximum, 15% less than that of the untreated cells, indicating the presence of a very slight delay in cell proliferation. Data

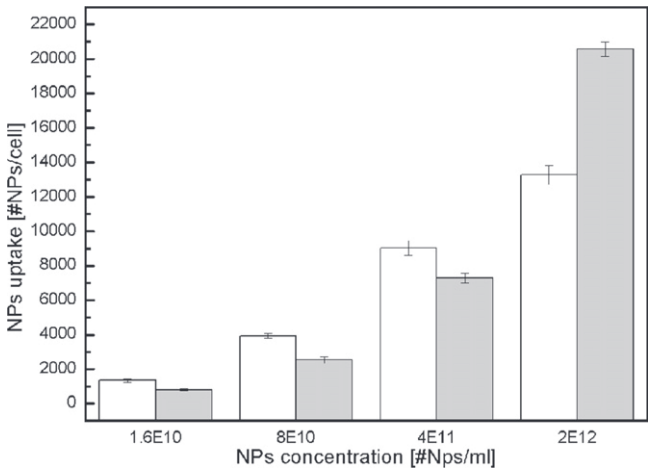

Figure 2. Quantification of the uptake of NPs by B16/F10 cells expressed as the average number of NPs per cell (#NPs/cell) after 1 h (white bars) and 24 h (grey bars) of incubation with different NP concentrations. The columns and error bars represent the mean and standard deviation of three replicates.

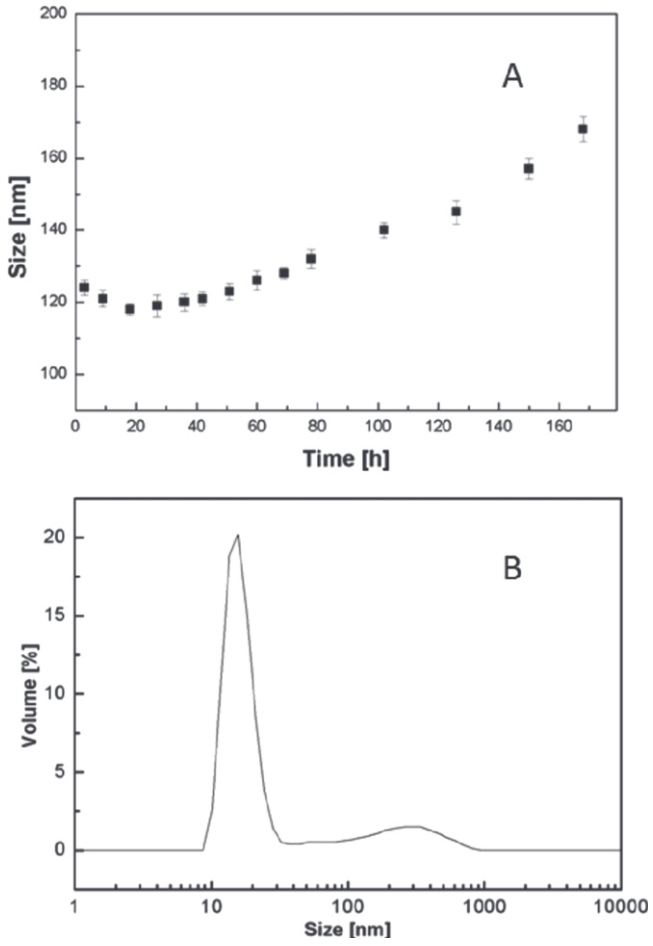

Figure 3. (a) Evolution of the diameter for the produced NPs in a cell medium at 37 °C, as determined by DLS measurements. (b) Particle size distribution of the degraded NPs after 160 h.

suggest that the cellular toxicity of these NPs could become an issue for prolonged exposure (24 h) with at least 10^{12} #NPs ml^{-1}.

The exploitation of the fluorescence signal of the RhB molecules covalently bound to the NPs and the application of the previously described analytical procedure [34], which involved the cellular uptake of the NPs after both 1 h and 24 h for all of the concentrations reported in figure 1, was studied. Cells were harvested at the indicated times and washed, and the NP concentration in the cellular sample was determined with a calibrated plate reader (see appendixes). In parallel, the cell concentration in the same sample was measured by a Coulter counter. The mean absolute number of NPs that were internalized into each cell was then estimated by dividing the NP concentration for the cell concentration. Obtained data as a function of time and NP exposure are reported in figure 2. For the lowest NP concentration (i.e., 1.6×10^{10} NPs ml^{-1}), about 1000 #NPs/cell are internalized (more specifically 1300 ± 100 #NPs/cell after 1 h and 800 ± 70 #NPs/cell after 24 h), while for higher concentrations, this value increases up to a maximum value of 20 000 #NPs/cell ($13\,000 \pm 500$ #NPs/cell after 1 h and $20\,500 \pm 400$ #NPs/cell after 24 h). It is important to notice that the NP uptake was very fast. The amount of internalized NPs reached relatively high values after 1 h and then decreased at 24 h, except for the highest NP concentration. Further experiments were made using time-lapse live-cell imaging in order to monitor the interaction between the cells and the NPs at very short times of incubation (figure E1 in the appendixes). Time lapse imaging confirmed that the NP uptake was fast; NPs were localized in the perinuclear region and reached a maximum concentration between 1 and 2 h.

3.3. Biodegradability: NP degradation in a cell medium

NP degradation has been followed in a cell medium at 37 °C through DLS measurements in order to study this process in a protein-rich environment.

In figure 3(a), the evolution of the diameter of the NPs is reported. The degradation of these NPs occurs through the hydrolysis of the ester bonds in the biodegradable PCL chains and through the subsequent release of the PCL oligomers [34].

A decrease in the NP diameter can be detected during the first hours of the experiments; this can be explained with the rearrangement of the PEG due to the change of the medium in which the NPs themselves are dispersed. As the hydrolysis occurs, the NPs become more and more hydrophilic due to the loss of CL units, which prompts an increase of the diameter due to the swelling process. Near the end of the degradation, the majority of the distribution of the degrading NP dimension (figure 3(b)) is mainly related to a peak at about 13 nm, which can be attributed to the residual poly (HEMA-g-PEG_{19}), which is organized into micelles (more information about the particle size distribution for shorter degradation times can be found in the appendixes). The

reliability of the timescale of this datum is confirmed by experiments in *in vitro* conditions, in which, 6 d after internalization into the cells, the same NPs cannot be detected anymore [31].

3.4. Biodistribution: in vivo studies

The good biocompatibility of the NPs, along with their ability to be internalized by B16/F10 mouse melanoma cells, fostered further *in vivo* studies of biodistribution.

RhB fluorescence was used to detect and quantify NPs during their time spent in different organs. The quantification was achieved using standard calibration curves of the NPs, characterized by a good linearity between the fluorescence and the NP concentrations (figure D1 in the appendixes). The determination of the fluorescence signal associated to a single NP in each organ or in the fluid allowed the assessment of NP concentrations at different times after injection. The detailed kinetics of the NPs in the plasma, liver and tumor are reported in figure 4. The NP concentration in plasma (panel A) decreases from the value expected on the basis of the assumed plasma volume (which corresponds to 151% ID/ml for the mice used in these experiments) to 5.6 ± 0.6% ID/ml in 24 h, falling below the limit of detection, which is around 0.03% ID ml^{-1} at 168 h. Data were properly fitted with a two-exponentials model, with a very rapid ($\tau_{1/2} = 0.5$ h) distribution phase followed by a slow ($\tau_{1/2} = 15$ h) elimination. This indicates that the majority of the NPs left the bloodstream in the first hour and were distributed to the main organs. The half-life of these NPs in blood is comparable with literature data for carriers stabilized with PEG chains of similar length [35].

As can be seen in figure 4(B), at 30 min post injection, the percentage of the injected dose per gram of tissue (% ID g^{-1}) in the liver was around half of the NP concentration in the plasma; these NP levels were not maintained for a prolonged time, and the NP concentration rapidly decreased in the first hour, as it did for the plasma. Differently from the plasma, where the NP concentration was continuously decreasing, the NP concentration in the liver reached an equilibrium value of around 2.5 ± 0.5% ID g^{-1} at 24 h, and then it was maintained for at least 7 d, up to the end of the observation time. Thus, while the majority of the NPs that initially reached the liver were eventually recycled to other districts or were excreted, a non-negligible fraction of them was stably incorporated within the organ, possibly intracellularly. The tumor instead was not reached immediately by the NPs (figure 4(c)), as a peak concentration was one order of magnitude lower than in the liver, but the NPs quickly reached a steady concentration of around 3 ± 0.4% ID g^{-1}. A leakage of NPs from the tumor seems apparent on the basis of the decrease of the NP concentration after 24 h. However, these tumors were rapidly growing, and their mass increase caused a dilution of the NPs in the tumor site. An adjustment of the data to account for the measured increase in tumor mass (figure 4(c), hollow circles) demonstrates that this effect fully explains the decrease of the NP concentration, and the overall number of the NPs in the tumor did not change significantly in the seven days of observation. Overall, NP accumulation in the tumor is consistent with the literature for the same tumor model and for similar carriers [36].

As reported in figure 5, steady NP concentrations in the tumor were similar to those in the liver, demonstrating the ability of these NPs to overcome biological barriers and to reach the target site, even in the absence of any additional functionalization to specifically target tumor cells. This can be done without excessively loading the liver with NPs, as the exposure of this organ to concentrations found to be slightly cytotoxic *in vitro* (above 1×10^{12} #NPs g^{-1}, which corresponds to 32% ID g^{-1}) was too short to produce cellular toxicity.

The time course in the kidney had a trend similar to that observed in the liver; it maintained relatively high levels of internalized NPs up to 72 h. A peculiar behavior was observed for the spleen, which trended toward an increase in the NP concentration, mainly because of a redistribution of residual circulating NPs. This confirms the effect already reported in literature [21, 37]. A possible role is also played by inflammatory processes induced by the B16 melanoma, which lead to spleen enlargement (not shown). In the lung and heart, the NP concentration was about one order of magnitude lower, while the absence of NPs in the brain confirmed that they were not able to cross the blood-brain barrier, as expected because of their size.

The analyzed organs represent a significant sample of all the injected NPs for only a few hours after injection; indeed, the sum of the recovered NPs (obtained by multiplying the NP concentration by the mass of the organs or the plasma volume) decreased down to about 12% of the total ID after 24 h. This value is substantially in agreement with results reported by Wenger *et al* for rats [38] and shows similar data for rapidly perfused organs. Figure 6 reports the overall amount of NPs retrieved in different organs and in the excreta. The latter was calculated by measuring fluorescence from feces and urines (figure 6) collected at 24 h and 72 h from mice maintained in metabolic cages. This accounts for the majority of the NPs excreted by the mice. At 24 h, the amount of NPs found in the feces and urines was respectively 65 ± 13% and 1 ± 0.9% of the ID. This fact confirms that the NPs are too big to be significantly filtered by the kidneys and consequently excreted by urine. Furthermore, the high NP presence in the feces highlights the role of the liver in the NPs' elimination, which mainly follows the hepatobiliary way.

Finally, data after the 72 h injection do not show a further significant increase of the recovered NPs. Including the NP amount in the feces and urine, the total amount (in terms of average value) of NPs detected was 77% of the total ID 24 h after injection, while after 72 h, this amount increased to the 86%. The remaining part of the NPs (i.e., 23% at 24 h and 14% at 72 h, in terms of average value) could be assumed to be cumulated into other tissues, muscles and bones, generally accounted as the carcass, which is not directly evaluable. Finally, the diminishment of the calculated value of the NPs into the carcass reveals the accumulation and the subsequent leakage of the NPs from these tissues, which can explain the increment of the NP

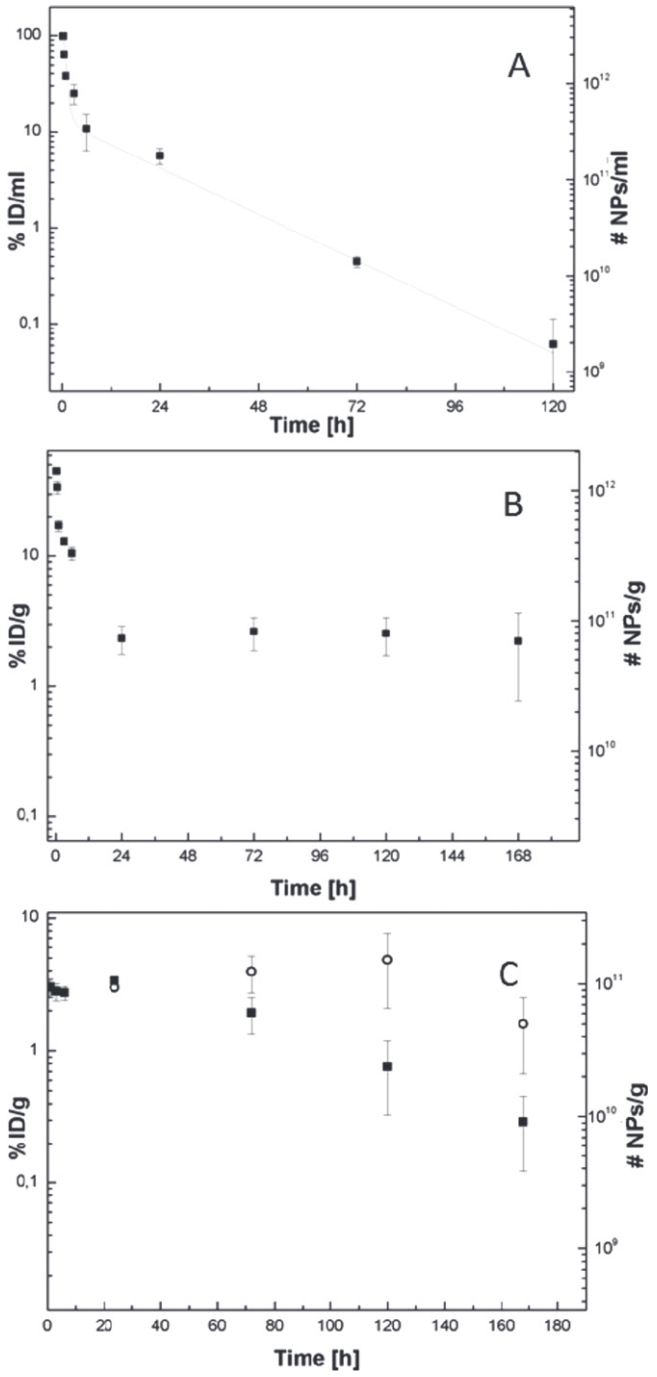

Figure 4. Time course of the NP concentration in the plasma (a), liver (b) and tumor (c) of C57BL/6 mice bearing the B16/F10 tumor. The values and error bars represent the mean and standard deviation of the measures in the three mice. The continuous line in panel A shows the best fit with a two-exponentials model. The tumor size was measured at each time with calipers (see experimental section), and the relative increase of the tumor volume was calculated. The hollow circles in figure 4(c) show the ratio between the measured tumor NP concentrations and the relative increase of the tumor size, giving a score proportional to the overall NP content in the tumor.

concentration in the spleen. In conclusion, the use of the RhB-based fluorescent monomer allowed in-depth *in vivo* studies, enabling the evaluation of the distribution of a

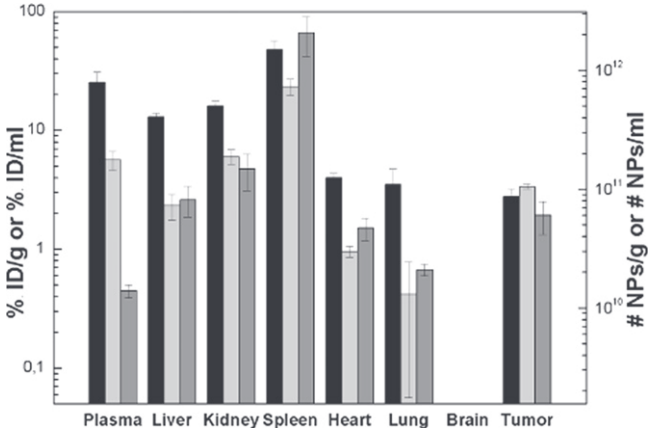

Figure 5. NP concentration in different organs calculated as a percentage of the injected dose per gram or ml (left scale) and the #NPs g^{-1} or ml (right scale). Data are taken at 3 h (black), 24 h (light gray) and 72 h (dark grey) after the injection. The values and error bars represent the mean and standard deviation of the measures in the three mice.

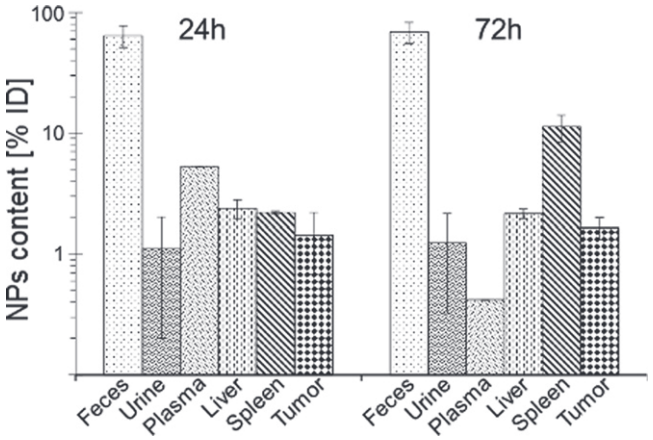

Figure 6. Overall NP content in different organs and the tumor, calculated as a percentage of the injected dose. The values and error bars represent the mean and standard deviation of the measures in the three mice.

significant fraction of the injected dose of the NPs, even after several days after injection.

3.5. Histological analysis

Histological analyses were carried out to determine where the NPs were localized inside the two main filter organs (liver and spleen) and in the tumor (figure 7). The green signal, related to the intrinsic autofluorescence of tissues, enabled us to visualize the structure of the parenchyma in the untreated mice and to better determine the distribution of the NPs in treated mice.

In the spleen, the signal associated with the RhB was exclusively found in splenic pulp (S.P) at 3 h (figure 7(b)), while at 72 h, a significant migration of the signal toward the lymphatic nodules (L.N) was observed (figure 7(c)). The merge between the Hoecsht 33 258 and the RhB (figure 7(d)) suggests an active

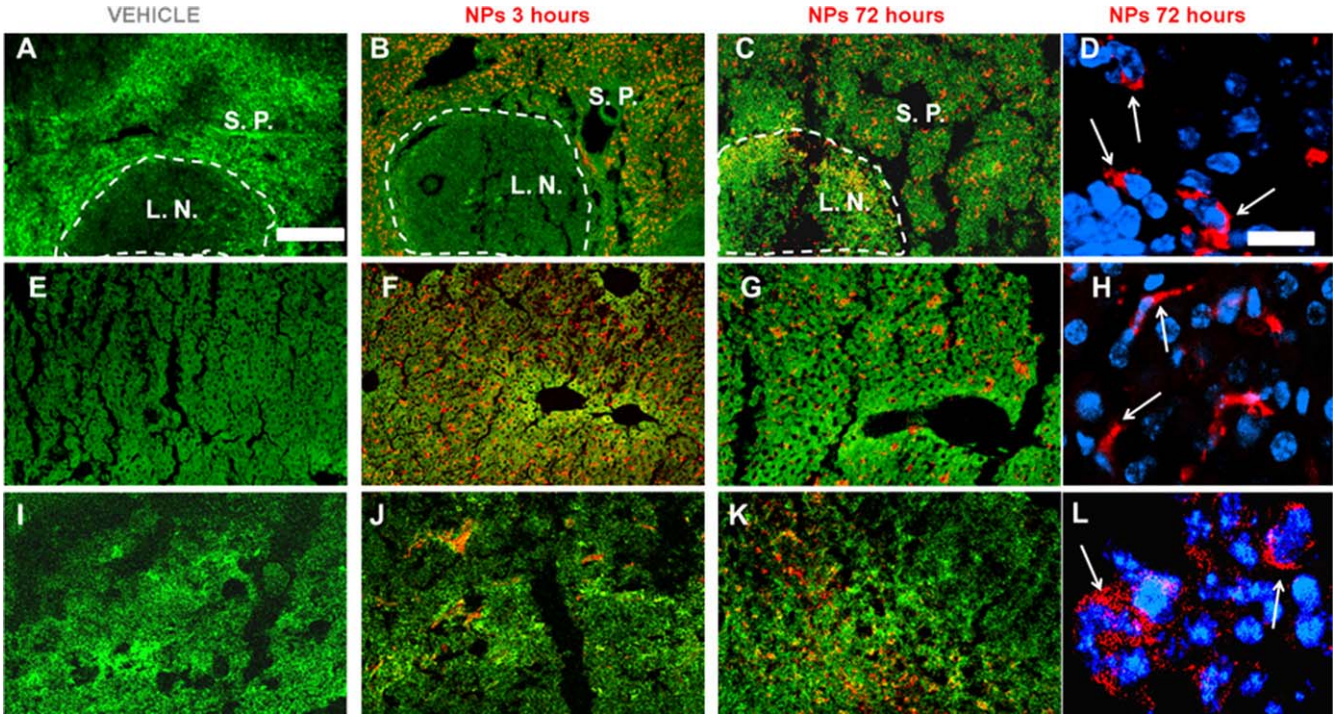

Figure 7. Representative microphotographs of the spleen (A)–(D), liver (E)–(H) and tumor sections (I)–(L) from the C57BL/6 mice bearing the B16/F10 tumor that were treated with saline solution (first left column) or sacrificed 3 h (second column) or 72 h (third and fourth columns) after the NP injection. The green staining is related to the autofluorescence of the tissues detected by exciting the sample by the laser with $\lambda = 488$ nm. The red staining is associated with RhB fluorescence, excited by the laser with $\lambda = 546$ nm. The overlap between the two signals is shown as orange-yellow staining. The fourth column depicts a higher magnification where the nuclei are stained blue with the marker Hoechst 33 258. Scale bar: (A)–(C), (E)–(G), (I)–(K) 200 μm, D, H and L 50 μm.

internalization of the NPs by the spleen cells (see arrows). An almost homogeneous signal associated with the RhB was instead observed in the liver at 3 h after NP injection (figure 7(f)), while at 72 h, the NPs were detected in small and localized areas (figure 7(g)). A higher magnified picture (figure 7(h)) confirms NP internalization in the cells (see arrows). In the tumor parenchyma, the autofluorescence signal reveals a disorganized structure (figures 7(i)–(k), green signals) where the NPs accumulated in selected areas (likely associated with tumor vessels) 3 h after administration (figure 7(j)). 72 h after the NP injection, a strong but heterogeneous increase of the red signal was observed in the tumor parenchyma (figure 7(k)). The double staining Hoechst 33 258-RhB highlights an efficient internalization in the tumor cells (figure 7(l)).

4. Conclusion

PCL-based NPs, constituted of a poly(HEMA) backbone grafted with PCL-chains of controlled length and PEG chains, have been produced by adopting a solvent and surfactant free process (MSSEP), and their stability in the condition of a biological interest (cell medium) has been proved. The NPs were tested in preclinical systems both *in vitro* and *in vivo* to determine their potential as drug delivery carriers. The biocompatibility of the NPs was tested *in vitro* by incubating B16/F10 cells for 24 h with different NP concentrations and showed no significant cytotoxicity, except for a very high NP concentration. These characteristics prompted us to test these NPs in *in vivo* experiments towards their development as a drug carrier. The NP injection in C57BL/6 mice bearing the B16/F10 tumor demonstrated that the latex was well tolerated by the animals, which were not affected by a significant decrease in body weight. The biodistribution experiment showed a fast decrease of the NPs in the plasma and liver in the first hour after injection ($\tau_{1/2} = 30$ min). After 3 d, NP accumulation was observed in the liver, spleen and tumor, while the majority of the NPs was already excreted via feces and urine. In particular, the NPs′ concentration in the tumor reached a steady level, showing significant long-term retention. Histological analyses demonstrated that the NPs were able to penetrate into the parenchyma of the tissues by a well-designed tropism and were efficiently internalized into tumor cells. The absence of cytotoxicity, the accumulation in the tumor and the fast excretions foster the development of the produced NPs as drug delivery carriers.

Acknowledgment

We acknowledge support from AIRC Special Program Molecular Clinical Oncology ‘5 per mille’.

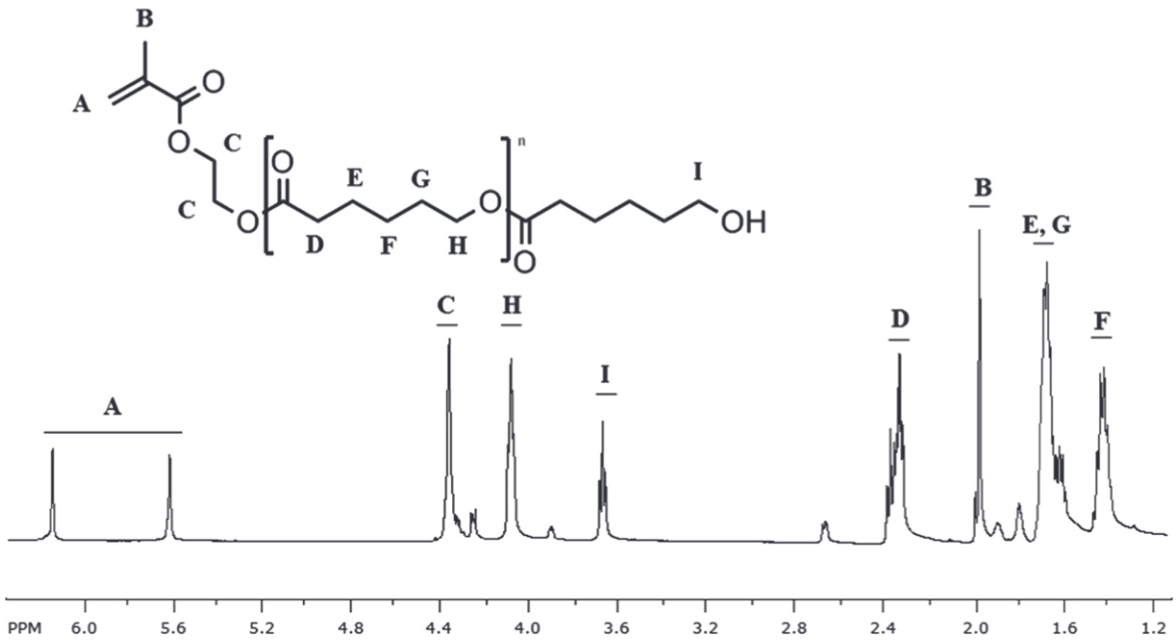

Figure A1. Spectrum for HEMA-CL_3.

Appendix A. ^{1}H-NMR spectra analysis

The ^{1}H-MMR analysis has been performed by dissolving the sample of the macromonomer in $CDCl_3$ and analyzing it in a 500 MHz apparatus (Bruker, Switzerland).

According to the reported spectra, the *Mn* of the material can be calculated as follows:

$$Mn = M_{HEMA} + M_{CL}\left[\frac{H\ (\text{methylene proton signal})}{I\ (\alpha\ \text{methylene proton signal})} + 1\right]. \quad (S1)$$

The term in brackets represents the average number of CL units that are attached at the HEMA molecule; and therefore, it is the main parameter that characterized all of the produced macromonomers and the NPs. It is derived as the ratio between the repeating CL units, H, and the terminal CL unit, I, which is then added to the total count. All of the area integrations have been made by setting the area of one of the vinyl hydrogen atoms of the HEMA group, A, as the unit.

Appendix B. NPs′ stability in cell medium

The stability of the produced NPs in a cell medium at 37 °C has been assessed via DLS measurements. In figure B1, the particle size distribution of the NPs before the contact with a cell medium after 1 h of testing and after 72 h of testing are reported.

As can be seen in the figure, there is a slight decrease in the NPs' diameter when the NPs are put in contact with a different medium, however, the absence of significant changes, both in terms of the average diameter and of the distribution width, rule out the possibility of NPs′ colloidal instability.

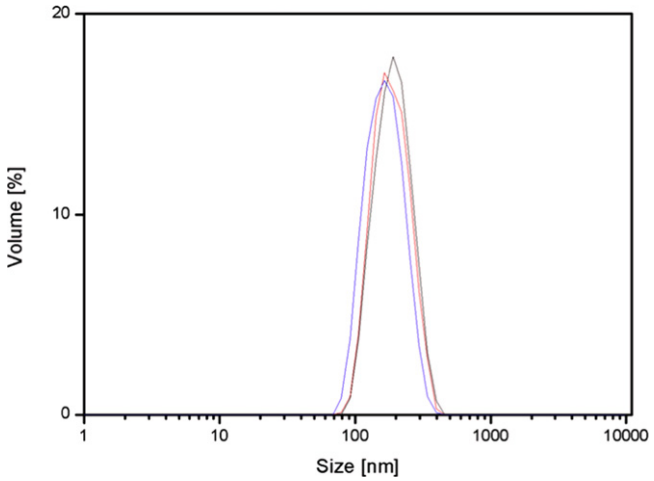

Figure B1. Evolution of the NPs′ size distribution: before contact with a cell medium (black line), after 1 h (red line) and after 72 h (blue line).

Appendix C. Cellular uptake, NPs′ concentration and calibration of the microplate reader

In order to standardize cell treatment in terms of NPs′ concentrations, the final latex solid content was converted into a number of NPs contained in each batch after the polymerization processes by using the following well-established relationship:

$$N_p = \frac{6\left[M_0\right]\chi_{cum}MW_{mon}}{\pi\rho_{pol}d^3}. \quad (S2)$$

Equation S2 allows us to relate the latex concentration with the number of NPs when the NPs′ diameter (d), starting monomer concentration ([M_0]), the conversion (χ), monomer MW (MW_{mon}) and polymer density are known (ρ_{pol}). Considering the extremely low amount of HEMA-RhB present in the final polymer (0.1% w/w) and the relatively low amount of degradable macromonomer, the pure PCL proprieties have been considered where required.

Since the amount of RhB fed during NPs′ synthesis is known, it is possible to calculate the amount of RhB (molecules or pmol) for each NPs′ concentration. Then, the calibrations of the microplate reader with the sequential dilutions of the NP batches with PBS or with specific tissue homogenates allow us to relate the measured fluorescence to the amount of the NPs or to the RhB content.

Appendix D. Standard calibration curves

Appendix E. Time-lapse

Time-lapse live-cell imaging was used to monitor NPs′ uptake at very short times of incubation. The B16/F10 cells were seeded in a μ-slide with 8 wells for immunofluorescence (Ibidi, Germany). 24 h after seeding, two different concentrations of NPs (40×10^{10} and 200×10^{10} #NPs ml^{-1}) were added, and the time-lapse measure was started. The image capture was controlled by cell^R software (Olympus, Germany), and all of the images were collected in phase contrast and in red fluorescence (λ_{exc}: 572/23 nm, λ_{em}: 628/28 nm) with an UPlanFLN 40x (Ph2) objective. Sequences were captured for one field for each well every 2 min for over 2 h. The Imaging Station cell^R (Olympus, Germany) used for the time-lapse experiment consisted of a IX81 motorized inverted microscope (Olympus); an incubator (OKOlab, Italy) to maintain optimal environmental conditions for cell growth,

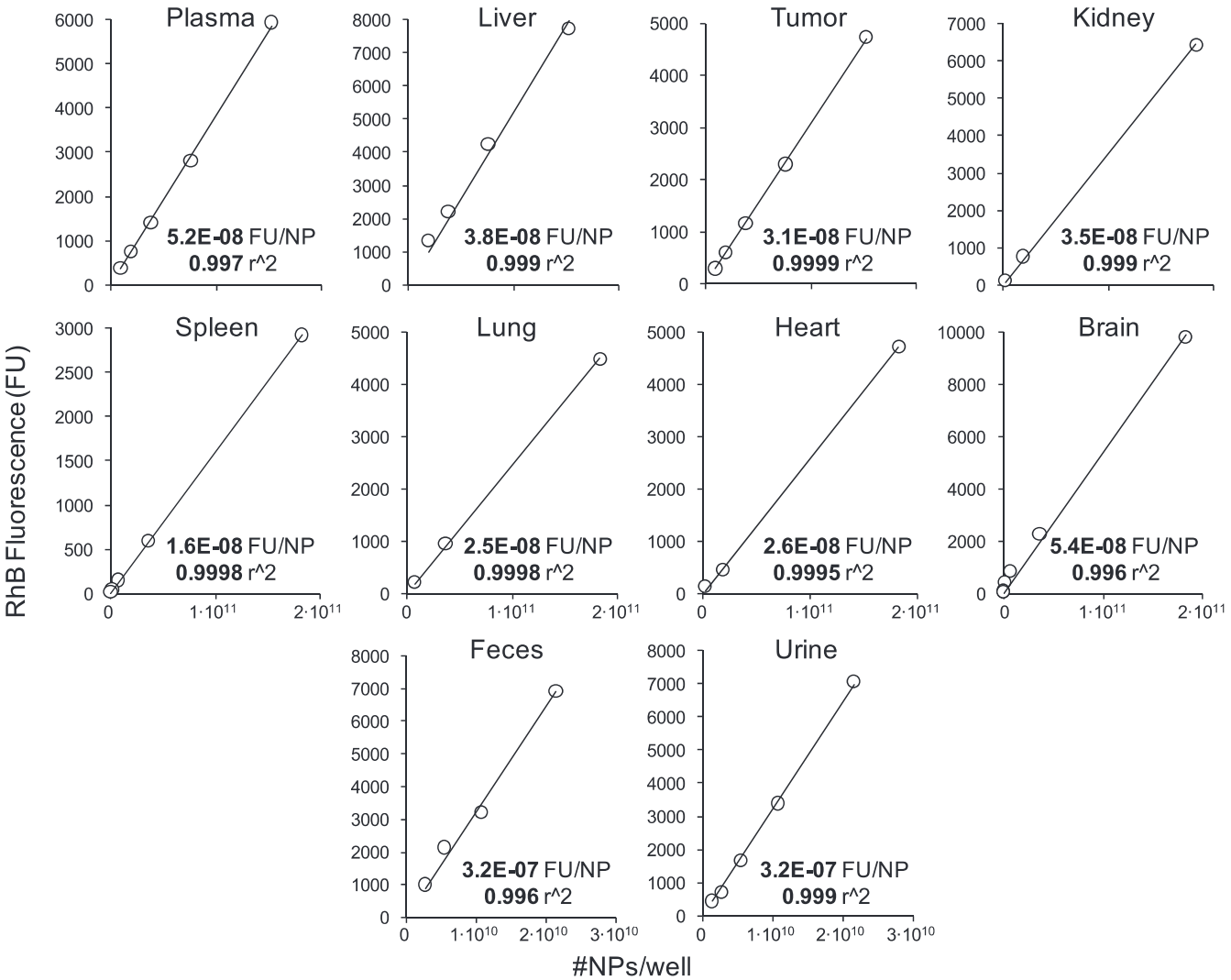

Figure D1. Linear fit of the microplate reader calibration curves obtained for each homogenized organ or fluid.

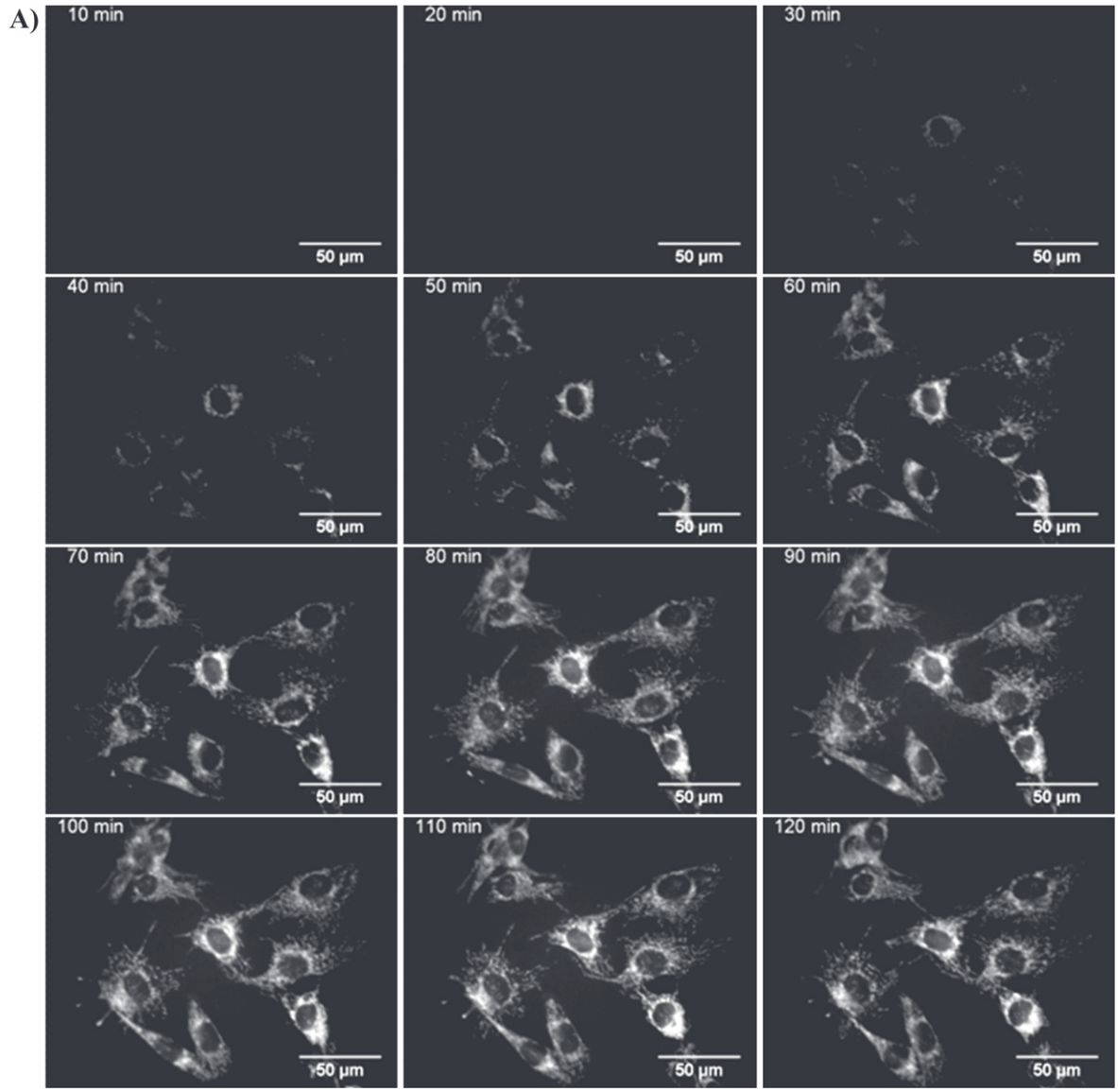

Figure E1. Image sequences obtained by time-lapse microscopy at the beginning of the incubation with NPs: (A) cells incubated with 40×10^{10} #NPs ml^{-1}. (B) Cells incubated with 200×10^{10} #NPs ml^{-1}. The brightness and contrast were kept constant within the A and B panels, with the brightness of sequence B lower than that in sequence A. The highest amount of NPs in the cellular medium caused a high background signal, and the reduction of brightness was necessary for better visualization of the time sequence.

temperature control, humidity and CO2; and an illumination system MT20, equipped with a 150 W Xe arc burner, ORCA-ER CCD camera (Hamamatsu, Japan) and X-Y positioning stage.

The aim of the time-lapse microscopy experiments was to monitor the time course of the NP uptake immediately after the NP addition. In the sample incubated with the lowest concentration (panel A), it was already possible 30 min after the NP addition to observe a fluorescence signal localized around the perinuclear region of the cells; this region rapidly increased. The internalization process was slower in the cells exposed to the highest amount of NPs (panel B), substantially confirming the trend observed by flow cytometric analysis.

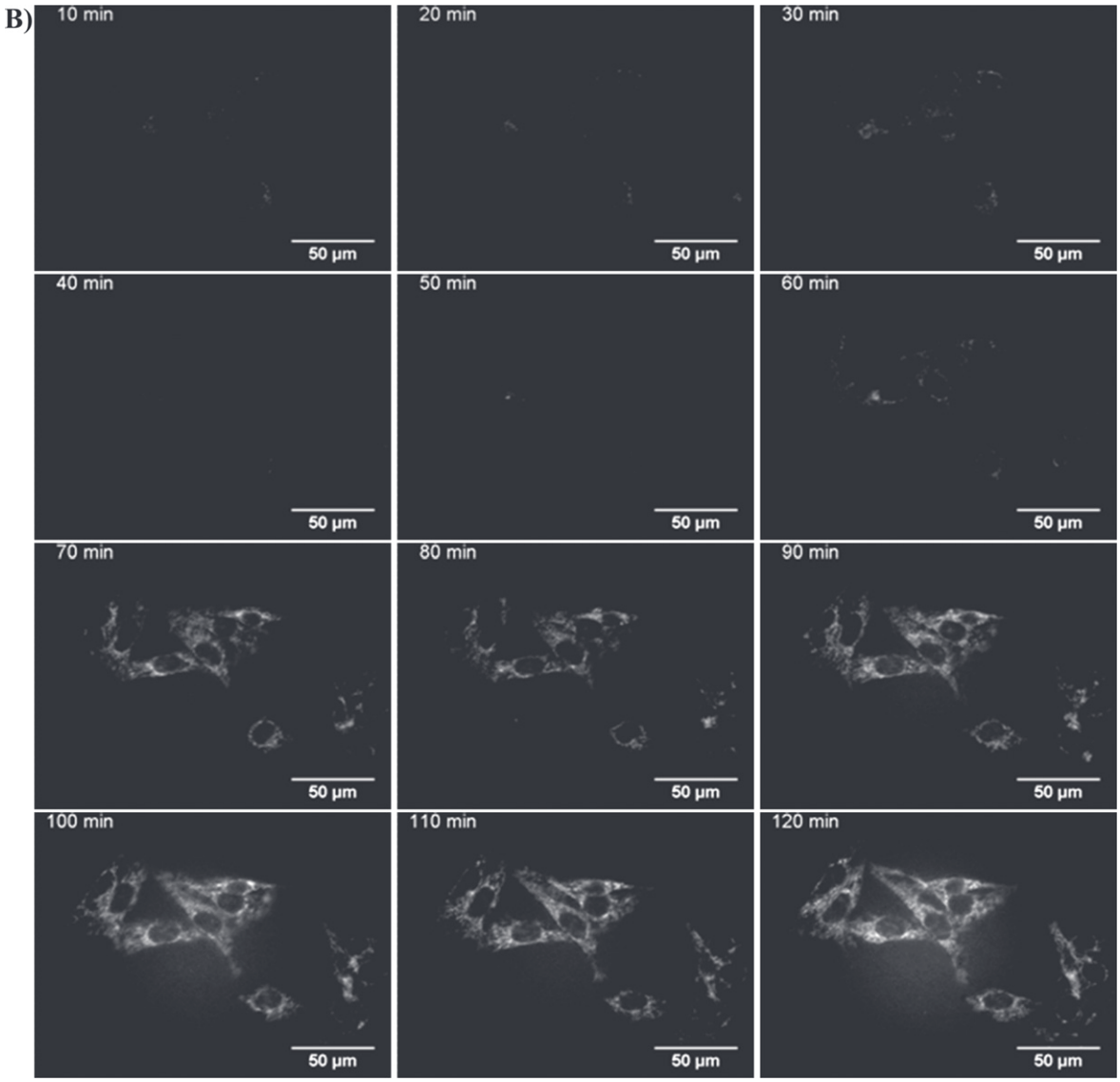

Figure E1. (Continued.)

References

[1] Davis M E, Chen Z and Shin D M 2008 *Nat. Rev. Drug Discov.* 7 771–82
[2] Kamaly N, Xiao Z, Valencia P M, Radovic-Moreno A F and Farokhzad O C 2012 *Chem. Soc. Rev.* 41 2971–3010
[3] Chaudhari K, Ukawala M, Manjappa A, Kumar A, Mundada P, Mishra A, Mathur R, Mönkkönen J and Murthy R R 2012 *Pharm. Res.* 29 53–68
[4] Kumar A, Chen F, Mozhi A, Zhang X, Zhao Y Y, Xue X D, Hao Y L, Zhang X N, Wang P C and Liang X J 2013 *Nanoscale* 5 8307–25
[5] Xiao K, Li Y, Luo J, Lee J S, Xiao W, Gonik A M, Agarwal R G and Lam K S 2011 *Biomaterials* 32 3435–46
[6] Amoozgar Z and Yeo Y 2012 *Wiley Interdiscip. Rev. Nanomed. Nanobiotechnol.* 4 219–33
[7] Zhang Z P, Lee S H and Feng S S 2007 *Biomaterials* 28 1889–99
[8] Gao F *et al* 2012 *Nanoscale* 4 3365–72
[9] Zhao P *et al* 2012 *Eur. J. Pharm. Biopharm.* 81 248–56
[10] Cirstoiu-Hapca A, Buchegger F, Lange N, Bossy L, Gurny R and Delie F 2010 *J. Control. Release* 144 324–31
[11] Liu Y T, Li K, Liu B and Feng S S 2010 *Biomaterials* 31 9145–55
[12] Tseng C-L, Su W-Y, Yen K-C, Yang K-C and Lin F-H 2009 *Biomaterials* 30 3476–85
[13] Goldmann E 1908 *Proc. R. Soc. Med.* 1 1–13
[14] Maeda H, Bharate G Y and Daruwalla J 2009 *Eur. J. Pharm. Biopharm.* 71 409–19
[15] Svenson S 2012 *Curr. Opin. Solid St. M.* 16 287–94
[16] Taurin S, Nehoff H and Greish K 2012 *J. Control. Release* 164 265–75
[17] Bae Y H and Park K 2011 *J. Control. Release* 153 198–205
[18] Alexis F, Pridgen E, Molnar L K and Farokhzad O C 2008 *Mol. Pharmaceutics* 5 505–15
[19] Dobrovolskaia M A, Aggarwal P, Hall J B and McNeil S E 2008 *Mol. Pharmaceutics* 5 487–95
[20] Sokolova V and Epple M 2011 *Nanoscale* 3 1957–62
[21] He C, Hu Y, Yin L, Tang C and Yin C 2010 *Biomaterials* 31 3657–66
[22] Davda J and Labhasetwar V 2002 *Int. J. Pharm.* 233 51–9

[23] Cartiera M S, Johnson K M, Rajendran V, Caplan M J and Saltzman W M 2009 *Biomaterials* 30 2790–8
[24] Shenoy D, Little S, Langer R and Amiji M 2005 *Mol. Pharmaceutics* 2 357–66
[25] Cheng J, Teply B A, Sherifi I, Sung J, Luther G, Gu F X, Levy-Nissenbaum E, Radovic-Moreno A F, Langer R and Farokhzad O C 2007 *Biomaterials* 28 869–76
[26] Bartlett D W, Su H, Hildebrandt I J, Weber W A and Davis M E 2007 *PNAS* 104 15549–54
[27] Lee H, Hoang B, Fonge H, Reilly R and Allen C 2010 *Pharm. Res.* 27 2343–55
[28] Ferrari R, Yu Y C, Morbidelli M, Hutchinson R A and Moscatelli D 2011 *Macromolecules* 44 9205–12
[29] Ferrari R, Yu Y, Lattuada M, Storti G, Morbidelli M and Moscatelli D 2012 *Macromol. Chem. Phys.* 213 2012–8
[30] Dossi M, Ferrari R, Dragoni L, Martignoni C, Gaetani P, D'Incalci M, Morbidelli M and Moscatelli D 2013 *Macromol. Mater. Eng.* 298 771–8
[31] Papa S *et al* 2013 *ACS Nano* 7 9881–95
[32] Ferrari R *et al* 2014 *Nanotechnology* 25 045102
[33] Lazzari S, Moscatelli D, Codari F, Salmona M, Morbidelli M and Diomede L 2012 *J. Nanopart. Res.* 14 1–10
[34] Ferrari R, Colombo C, Casali C, Lupi M, Ubezio P, Falcetta F, D'Incalci M, Morbidelli M and Moscatelli D 2013 *Int. J. Pharm.* 453 551–9
[35] Gaucher G V, Asahina K, Wang J and Leroux J-C 2009 *Biomacromolecules* 10 408–16
[36] Rossi J, Giasson S, Khalid M N, Delmas P, Allen C and Leroux J-C 2007 *Eur. J. Pharm. Biopharm.* 67 329–38
[37] Malfatti M A, Palko H A, Kuhn E A and Turteltaub K W 2012 *Nano Lett.* 12 5532–8
[38] Wenger Y, Schneider I R J, Reddy G R, Kopelman R, Jolliet O and Philbert M A 2011 *Toxicol. Appl. Pharm.* 251 181–90